3D Acoustic imagery generation by interferometric analysis of long baseline using Interferometric Real Aperture Sonar.

Mitsuhiro Kojima
Akira Asada
Katsunori Mizuno
Fuyuki Katase
University of Tokyo 3-8-1 Komaba, Meguro-ku, Tokyo 153-8902 JAPAN
mkojima@iis.u-tokyo.ac.jp
asada@iis.u-tokyo.ac.jp
kmizuno@iis.u-tokyo.ac.jp
fkatase@iis.u-tokyo.ac.jp

Aritoshi Mio
NTT DATA CCS 4-12-1 Higashishinagawa, Shinagawa-ku tokyo JAPAN
amio@nttdata-ccs.co.jp

Satoshi Tsukioka
Shinobu Omika
JAMSTEC 2-15, Natsushima-cho, Yokosuka-city, Kanagawa 237-0061 JAPAN
tsukiokas@jamstec.go.jp
omika@jamstec.go.jp

Tamaki Ura
Kyushu Institute of Technology 1-1 Sensui-cho, Tobata-ku, Kitakyushu-shi, Fukuoka 804-8550 JAPAN
ura@iis.u-tokyo.ac.jp

***Abstract*—We are developing a technique for the systematical exploration of submarine hydrothermal ore deposits. In the Izu-Ogasawara Arc area these deposits are usually characterized by the existence of tower-like vents 2~20m high by 2~5m wide. We are using a set of Interferometric Real Aperture Sonars (InRAS) to generate 3D acoustic images of the areas surrounding the vents. We not only improved the resolution thanks to a long interferometric baseline, but we also efficietnly unwrapped the phase in this zone of large elevation differences by applying a two-stage approach (Branch Cut and SSPU methods). These improvements allow us to map the seafloor bathymetry around the submarine hydrothermal deposits. Since April 2014 we are conducting in-situ observations of both known and potential zones of hydrothermal deposits. Moreover, in November 2015 we will gather validation data in an experimental pool.**

Keywords— Interferometric Real Aperture Sonar; bathymetry; Hydrothermal deposits; Phase unwrap

I. Introduction

As part of the marine mineral resources development project of the Japanese Ministry of Education, launched in 2013, we have been developing a set of technologies for the exploration of submarine hydrothermal ore deposits. The aim of this national project is to systematize the exploration of hydrothermal deposits using several approaches shown in Fig.1. This paper focuses on the third method "High Resolution 3D Acoustic Imaging". The discovery of submarine hydrothermal deposits with this method is eased by the detection of hydrothermal vents and the acquisition of the bathymetry which reflects the nature of the substratum around the vents. Our final goal is to develop a technique that would automatically delimitate hydrothermal deposits from the data gathered with an Interferometric Real Aperture Sonar (InRAS). However, our immediate goal is to achieve the acoustic mapping of the seafloor with a resolution of about 30cm using InRAS.

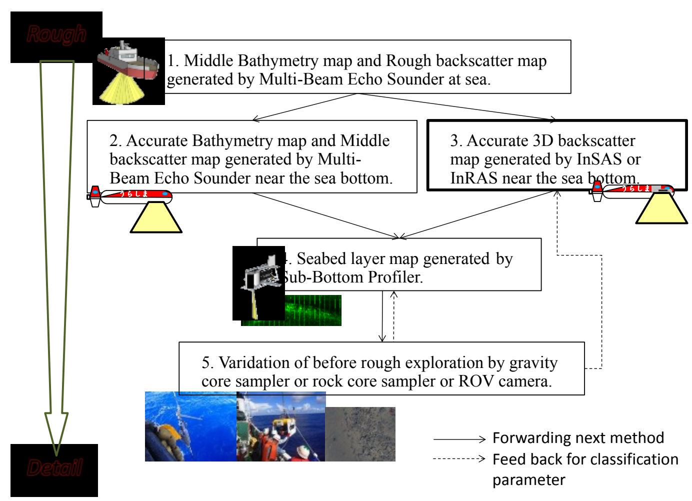

Fig. 1 Exploration techniques for the identification of hydrothermal deposits

II. Equippments

A. Interferometric Real Aperture Sonar

InRAS is an active sonar: a transmitter (Fig.2) emits acoustic waves like a side scan sonar, which the seafloor backscatters, and an array of receivers (Fig.3) retrieves the echo. Fig.4 shows the overall arrangement. One sonar is comprised of one transmitter and two arrays of receivers, each array having 24 hydrophones (12-channel × 2 rows). With one sonar on each port side there is a total of 96 hydrophones.

This is a DRAFT. As such it may not be cited in other works. The citable Proceedings of the Conference will be published in IEEE Xplore shortly after the conclusion of the conference.

However, because the path difference of the acoustic wave emitted in a direction perpendicular to the traveling direction determines the interferometry, an interferogram is generated by two pairs of four channels, for instance ch1,ch13, ch25, and ch37. In our study it is therefore possible to generate six (${}_4C_2$) interferograms per two pair of hydrophones.

Fig. 2 Transmitter

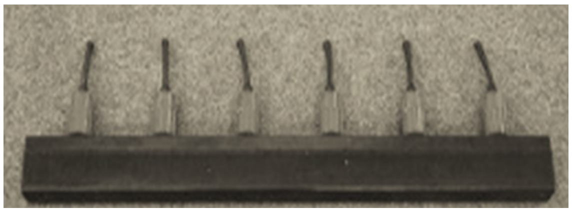

Fig. 3 Receiver (hydrophones)

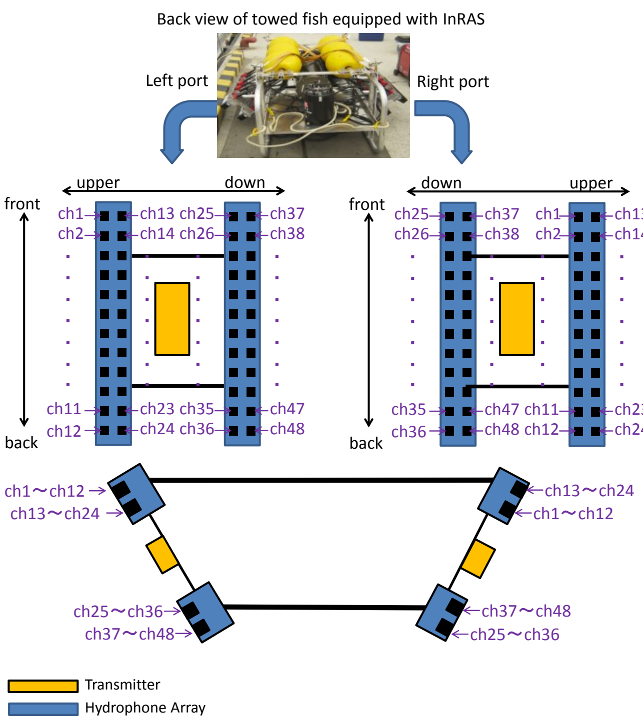

Fig. 4 Arrangement of the transmitters and receivers.

B. Autonomous Underwater Vehicle

InRAS-based surveys have been performed by loading sonars onboard an AUV named Urashima, developed and operated by the JAMSTEC (Japan Agency for Marine-Earth Science and Technology). Its specifications are given in Table 1. The payload included other devices (DVL, CTD, etc.) beside the sonar.

Table. 1 Specifications of AUV Urashima.

item	*Specification*
Max depth	3,500 m
Cruising distance	100 km (with Li-ion Battery)
	300 km (with Fuel Cell Battery)
Size	10m x 1.3m x 1.5m (L x W x H)
Energy source	Li-ion Battery or Fuel Cell Battery
Mode of Operation	autonomous navigation and remote control
Payload	CTD, DVL, ADCP, Multi beam echo sounder, Sub bottom profiler, etc.

C. Observation system

Urashima is operated during the survey so as to navigate at a speed of 1.5 knots 60~100m above hydrothermal deposits as show in Fig.5. The AUV has a dual navigation mode, either constant depth or constant elevation above seafloor. The former is suitable for synthetic aperture processing because the AUV has a uniform motion. The latter is suitable for interferometric processing with constant interferences as the elevation to the seafloor does not change. During the present study we used the constant depth mode because we were lacking sufficient bathymetry data to achieve the navigation in constant elevation mode.

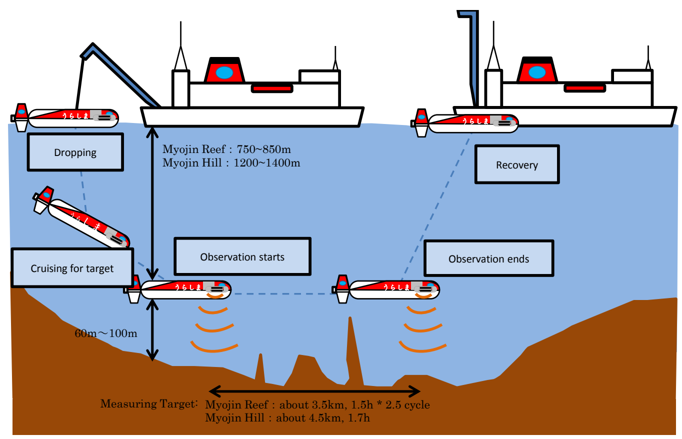

Fig. 5 InRAS-based observation procedure.

III. Methodology

Fig.6 is the flowchart for the generation of 3D acoustic images from the data which InRAS gathered. The sound velocity is derived from the empirical formula [2], the salinity, temperature and depth. Temperature and depth were recorded with the CTD. Salinity is derived from the empirical formula [1] and the electric conductivity that the CTD also recorded.

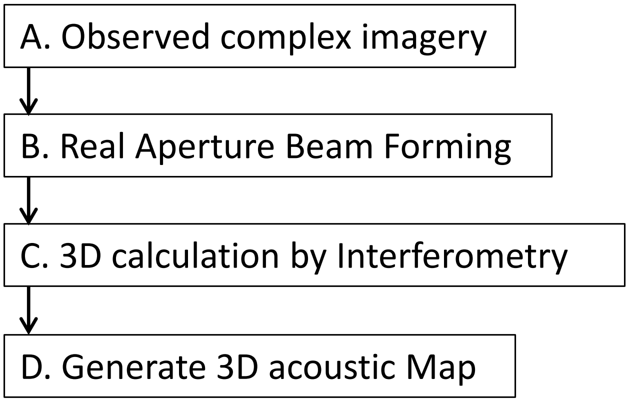

Fig. 6 Flow to generate 3D acoustic Map.

A. Observed complex images

Table 2 provides the specifications for the processing of the observation data.

The raw observation data were decimated by selecting specific frequencies, and stored as complex data. In fact, we reduced the amount of data to store by applying a DFT (Discrete Fourier transform) to the raw waveforms, and selecting only the frequency components that we are interested in.

We wanted to use a frequency of observation of 100KHz but in order to prevent interference between the AUV's starboard and port sides, the transmission-reception frequency was set to 93,750 Hz (right port) and 109,375 Hz (left port), respectively.

Table. 2 Specifications for the processing of the raw data.

item	***Specification***
DFT window size	32 samples
DFT interval	32 samples
AD converting rate	500,000 Hz
Sampling Freq	1,000,000 Hz (λ≒4.8 cm)
Thinned Sampling Freq	31,250 Hz
Ping cycle	0.5 sec
Number of samples at 1 ping	12500 samples (≒300 m)
Output data size	2byte real and imaginary
Output Freq	Left Port: 109,375 Hz Right Port: 93,750Hz

B. Real Aperture Beam Forming

Synthetic aperture beamforming in the azimuth direction usually involves range migration and the resulting Doppler effect. However, in the case of InRAS, we assume that the effect of range migration is very weak because the acquisition channels are spaced by less than 10cm. In addition, we equally ignore the Doppler effect because of the slow speed of AUV (1.5 knots). Consequently, in this study beamforming is achieved by simply stacking in the traveling direction the data of the 12 channels.

C. 3D Calculation by Interferometry

The flowchart for the interferometric processing is described in Fig.7.

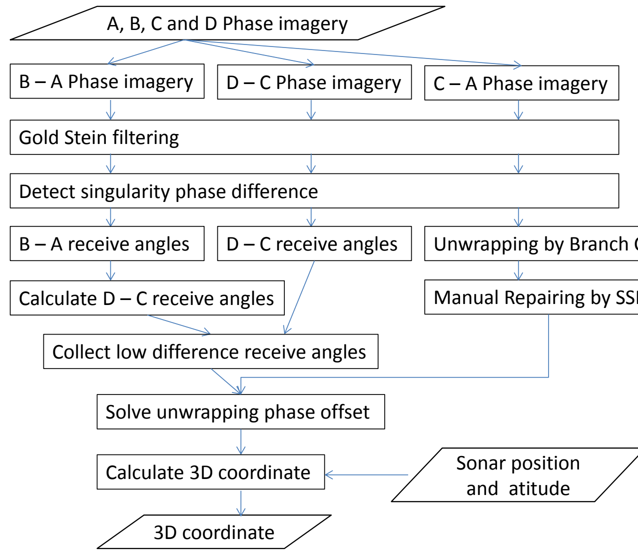

Fig. 7 Processing flow

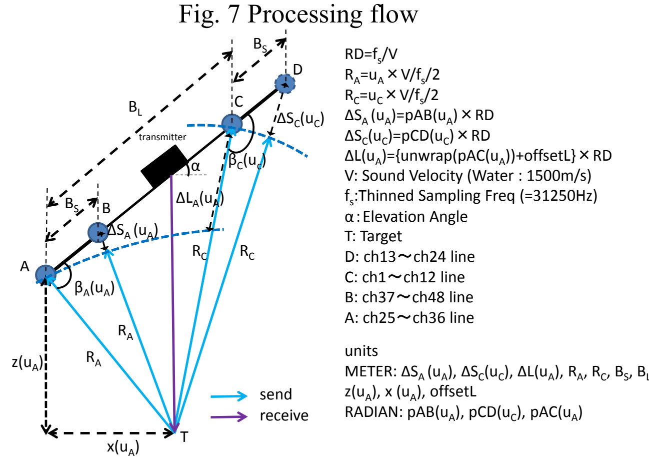

Fig. 8 Relative geometry of the phase difference and sonar.

a) Computation of the phase difference and filtering

Fig. 8 represents the geometry of observation for the starboard side InRAS, as seen from the AUV's rear. Let's determine the phase difference for three short baseline pairs *BA*, *DC*, and *CA*, where *A*~*D* correspond to the successive position of the receiving channels. Because the phase contains speckles due to multiple scattering and electrical interference, we removed the noise in the interferograms using a frequency filter, namely a Goldstein filter[4] with the following parameters: window size 64x64 pixel, processing interval 32 x 32 pixel, □ = 0.85. These values were determined heuristically as the lower limits above which unwrapping does not generate errors and discontinuities. The phase differences after filtering for the pairs *BA*, *DC*, *CA* are called $pBA(u_A)$, $pDC(u_C)$, $pCA(u_A)$, respectively. u and its subscript represent the pixel value in the range direction, and the receiving channel, respectively..

b) Unwrapping

Unwrapping consists in unfolding the phase difference which is wrapped in the interval 0 ~ 2π. In the present study, we used the Branch Cut method[3][4]. It operates by masking in an interferogram either the noisy areas or those of low phase continuity, then process only the areas of high phase continuity. At first, it sums in a clockwise rotation around a pixel of reference the phase difference of four neighboring pixels, as shown in Fig.10. The total amounts 0 when the phase changes gently, 1 or -1 otherwise.±1 is called residue[5]. Unwrapping when a residue is likely to occur yields different outputs depending on the direction of summation, so the solution is not uniquely determined (Fig.11). Branch Cut ties together the ±1 points to delineate masking areas that will not be unwrapped, representing a shortest distance.

Fig.9 shows the phase fringes for two baselines *BA* (left) and *CA* (right). The difference is related to the length of the baseline. Unwrapping for baseline *CA* is formalized as follows.

$$apCA(u_A) = unwrap(pCA(u_A)) + offsetL$$

offsetL represents the phase difference of the reference point when unwrapping. Then to unwrap for *BA*, it is possible to obtain the absolute phase difference ($apBA(u,v) = pBA(u,v)$) without unwrapping because the phase difference $pBA(u, v)$ falls within one fringe.

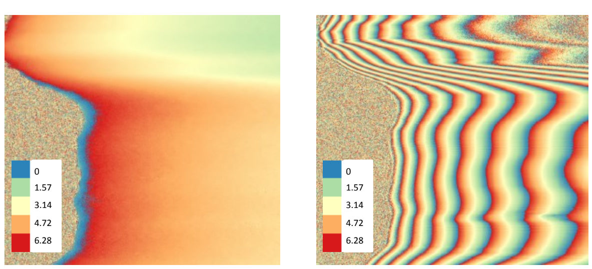

pBA(u_A) phase difference imagery pCA(u_A) phase difference imagery

Fig. 9 Impact of the baseline on the interferometric fringes (Start point is upper left;Vertical axis: azimuth, Horizontal axis: range).

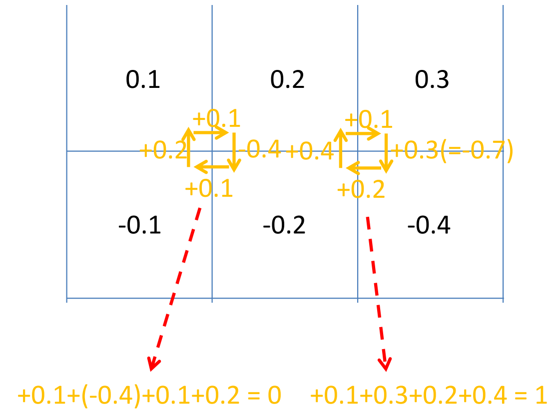

Fig. 10 Summing phase differences in an interferogram

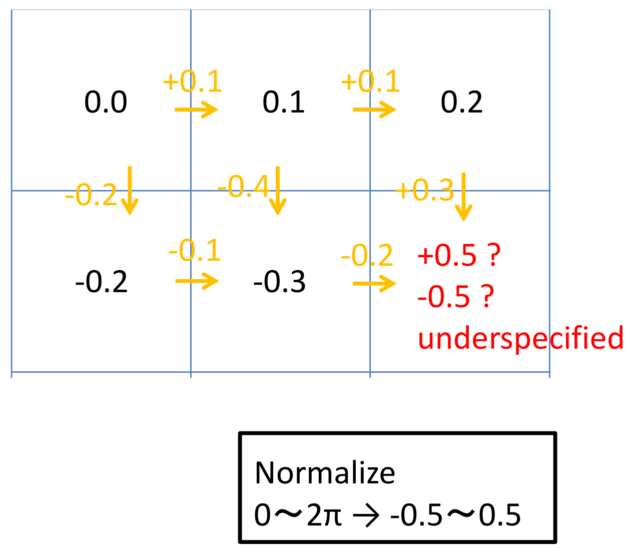

Fig. 11 Summing phase differences around phase singularity

c) Partial modification of the unwrapping ouput

The purpose of Branch Cut is to avoid unwrapping errors by masking residues, but it happens that large phase differences generate residues so that unwrapping errors are unavoidable. Therefore, phase singularity is very likely to occur since our study is targetting hydrothermal vents characterized by sudden differences in elevation. Thus we adopted the Singularity-Spreading Phase Unwrapping method ((hereinafter SSPU[6]), a technique that does not significantly disturb the phase change around singularities. SSPU minimizes as much as possible the value of all phase singularities by constantly removing an equal amount of the phase difference at one point to its four or more adjacent surrounding neighbours. However, because this process is lengthy when applied throughout the interferogram, instead we selected target regions from power images and applied SSPU to these specific areas. Then we combined them to the same areas that were Branch Cut-processed, using the least-squares method.

d) Computing and selecting the angles of arrival of backscattered signals

The angles of arrival β_A and β_C (Fig.8) are determined by applying the cosine theorem to the edges of triangles □*BAT* and □*DCT*. Because we want to compute B_L, R_A, and β_A in □*CAT*, it is possible to determine R_C from the cosine theorem. The length *DC* is computed the same way. Therefore, it is possible to compute $\Delta S_C(u_A)$ relatively to $\Delta S_A(u_A)$, and find $\beta_C(u_A)$ using the cosine theorem. $\beta_C(u_A)$ as determined by calculation and $\beta_C(u_A)$ as obtained from $pDC(u_C)$ are in theory equal when the relation $u_c = u_a$ is satisfied. In order to satisfy this condition we determine $\beta_C(u_C)$ from $\beta_C(u_A)$ by interpolating between two values of R_C: one computed from $\beta_A(u_A)$ and the other obtained from $\beta_C(u_C)$. By assigning a threshold (*Nrad*) to the difference of angles of arrival it is possible to select only high precision angles.

$$\beta_C(u_C)'ug\ \beta_C(u_C) < Nrad$$

The value of Nrad is equivalent to the highest resolution in arrival for a baseline length B_L.

e) Computing the offset caused by unwrapping, and the angle of arrival for long baselines

The offset that the unwrapping process generates can be expressed by the following equation.

$$offsetL = \Delta L(u_A) \,/\, RD - unwrap(pAC(u_A))$$

We compute $\Delta L(u_A)$ with the cosine theorem on the edges of □*CAT*, and by using the previous angle of arrival $\beta_A(u_A)$. The final offsetL is obtained as follows by averaging each channel.

$$offsetL = \Sigma\{\Delta L(u_A) \,/\, RD - unwrap(pAC(u_A))\} \,/\, N$$

And, we recomputed $\beta_A(u_A)$ from offset, unwrap($pAC(u_A)$), and *BL*. Incidentally, when determining $pAC(u_A)$ it is possible to mask the pixels with phase singularities to remove the noise.

f) Computing 3D data

We determine θ, the angle of arrival relative to the horizontal axis, by subtracting α, the setting angle of the sonar, to the angle of arrival $\beta_A(u_A)$. Then, from θ we obtain the following coordinates.

$$X(u_A) = R_A \times \sin\theta$$

$$Z(u_A) = R_A \times \cos\theta$$

Finally, the cross product of the coordinates of the sonar with its orientation yields the geographical coordinates.

D. Generating 3D acoustic Map

3D acoustic images are generated from the spatial coordinates (III.C) and power images derived from the complex images (III.A), and after performing some rendering. Rendering, a computer graphics technique, generates stereoscopic two-dimensional images from arbitrary viewpoints and angles.

IV. RESULTS

The technique described above has been used to process data collected in October 2014 on Myoujin calddera, Izu-Ogasawara Arc, Japan. In Fig. 12 to 15 the upper left corner is the origin, and the vertical and horizontal axes represent the traveling and range directions, respectively. Fig. 12 shows, on the left, the power image obtained from the complex data created in step III.A, and on the right, the same image after beam forming (III.B). It is clear that the resolution improves in the traveling direction.

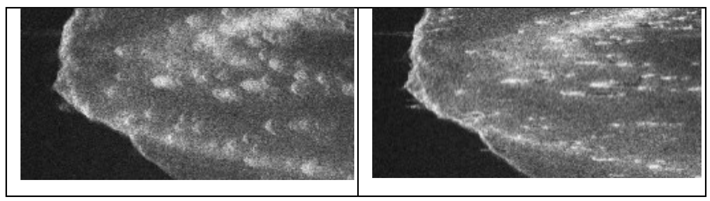

Fig. 12 Power image before and after beam forming (left: 1channel; right: stacking of channels 1-12)

The effect of the Goldstein filter is shown in Fig. 13. It confirms that this filter efficiently removes the speckle-like noise. Fig. 14 shows the same data before and after Branch Cut processing. It is clear that with the exception of a few noisy areas the scene is mostly unwrapped. Fig. 15 shows that SSPU can be used to efficiently compensate the errors that Branch Cut-based unwrapping generated.

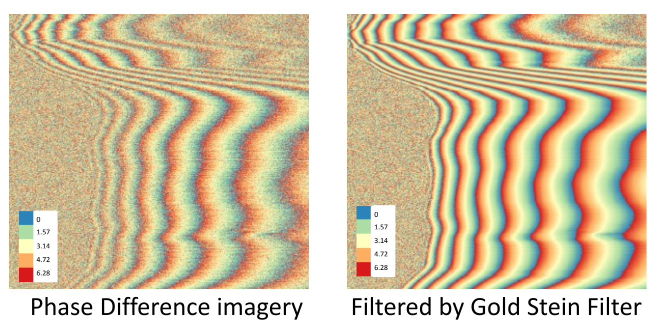

Fig. 13 Interferogram before (left) and after (right) filtering with a Goldstein filter.

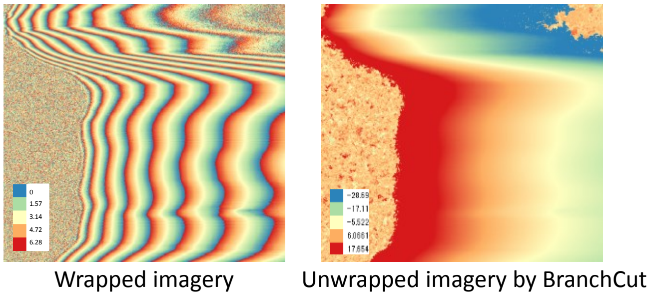

Fig. 14 Interferogram before (left) and after (right) Branch Cut.

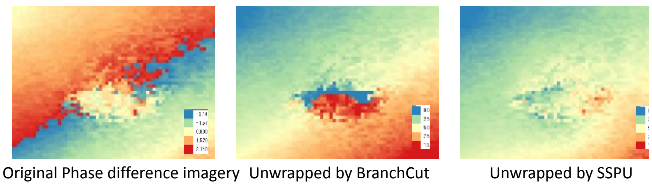

Fig. 15 Comparison between Branch Cut and SSPU.

Finally, applying the procedure that III.D described we generated 3D acoustic images (Fig. 17, right) from both the spatial bathymetry (Fig. 16, left) created in III.C, and power images (Fig. 16, right) obtained in III.B. Beside, the left hand side of Fig. 17 represents the 3D acoustic image ontained with pAB(u_A) values given (III.C) a short baseline.

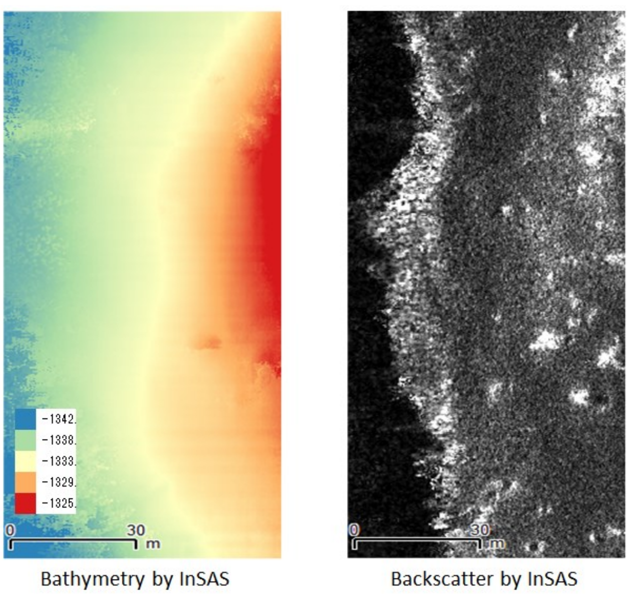

Fig. 16 Generated bathymetry (left) and power image (right)

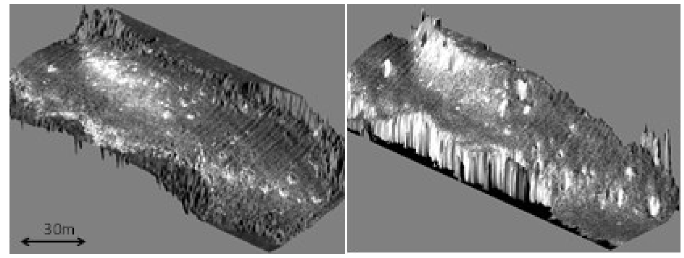

Fig. 17 InRAS-based 3D acoustic image.
Left:Short baseline(0.80λ), right: Long baseline(16λ)

V. CONCLUSION

We believe from the results of this study that long baseline interferometry and a combination of Branch Cut and SSPU unwrapping methods are suitable for generating elevation maps of the seafloor in the vicinity of hydrothermal deposits. This approach will be quantitatively evaluated in November 2015 by measuring the known position and size of a set of targets placed in an experimental pool. Though the present paper does not address this matter this experience will also be an opportunity to study the possibility of synthetic aperture.

Further developments will focus on the following three issues:

- Error in range with the shift of position of the sonar.

- Improving the accuracy of mounting of the sonar (position and angle).

- Improving the accuracy of position when generating interferograms.

ACKNOWLEDGMENT

I am deeply grateful to Japanese Ministry of Education. And, YOKOSUKA(JAMSTEC's ship) shipman's support were invaluable.

REFERENCES

[1] Unesco/SCOR/ICES/IAPSO Joint panel on Oceanographic Tables and Standards and SCOR Working Group 51, "Algorithms for computation of fundamental properties of seawater", Unesco technical papers in marine science, http://www.jodc.go.jp/info/ioc_doc/UNESCO_tech/059832eb.pdf (Accessed : 13/08/2015)

[2] C.T.Chen and F.J.Millero, "Speed of sound in seawater at high pressures", J.Acoust. Soc. Am., 62(5), 1129-1135(1977).

[3] R. M. Goldstein, H. A. Zebker, and C. L. Werner, "Satellite radar interferometry: two dimensional phase unwrapping," Radio Sci. 23, 713–720 (1988).

[4] Goldstein, R. and Werner C.: Radar interferogram filtering for geophysical application. Geoph. Res. Letters, Vol. 25, No.21, pp. 4035-4038, 1998.

[5] YUN Jun, Zhi-nong Zou, Jin-song TANG, Ai-qing WANG, “Experiment of Phase Unwrapping Algorithm in Interferometric Synthetic Aperture Sonar”, Eighth ACIS International Conference on Software Engineering, Artificial Intelligence, Networking, and Parallel/Distributed Computing, 937-941, 2007

[6] Ryo Yamaki and Akira Hirose, “Singularity-Spreading Phase Unwrapping”, IGARSS, 3240-3251, 2006